Nonergodicity of point vortices

Jeffrey B. Weiss and James C. McWilliams
National Center for Atmospheric Research, P.O. Box 3000, Boulder, Colorado 80307

(Received 10 September 1990; accepted 22 January 1991)

The motion of N point vortices in a two-dimensional fluid is a Hamiltonian dynamical system with a $2N$-dimensional phase space. The equations of motion for point vortices in a two-dimensional square doubly periodic domain are derived from those for an open domain. The Hamiltonian has three known constants of the motion and is thus believed to be nonintegrable for four or more vortices. Trajectories are numerically integrated from several initial conditions containing six vortices with varying total energy. Ergodicity on the surface defined by the constants of the motion is directly tested by comparing time-average and ensemble-average vortex pair statistics. It is found that the dynamics is not ergodic. There is evidence that the nonergodicity is not due to a gross fragmentation of phase space as might result from a broken symmetry. Vortex pair statistics are also used to test the randomness of the chaotic motion. It is found that the time-averaged statistics of the vortices are clearly distinct from those of independent random walkers.

I. INTRODUCTION

Hamiltonian dynamics describes the motion of physical systems in terms of trajectories in a d-dimensional phase space. Very low-dimensional Hamiltonian dynamics, that which can be reduced to a four-dimensional phase space with a conserved energy, has been the focus of intensive investigation in recent years.[1,2] As a result, there is now a clear understanding of chaotic and regular regions, KAM curves, cantori, and the diffusion of trajectories in phase space. In such systems it is known that KAM curves, two-dimensional tori, can divide the three-dimensional energy surface yielding nonergodic behavior. Time averages then depend on the initial condition of the trajectory. In higher dimensions, KAM tori do not divide the energy surface. Motion around these tori, called Arnold diffusion, makes it possible for trajectories to be ergodic. Very high-dimensional Hamiltonians, e.g., a macroscopic volume of gas where $d \sim 10^{23}$, are the subject of statistical mechanics,[3] where ergodicity is usually assumed. In this work the focus is on the middle ground, Hamiltonian dynamics in a moderate dimensional phase space, where we numerically test whether the dynamics is ergodic.

The system studied here is a collection of N point vortices in a two-dimensional fluid with doubly periodic boundary conditions. The dynamics of N point vortices is a $2N$-dimensional Hamiltonian system. The point vortex Hamiltonian is thought to be nonintegrable for $N \geqslant N^*$ where N^* depends on the geometry of the system.[4] For a square doubly periodic domain, $N^* = 4$. Unlike the near-integrable Hamiltonians often studied, the point vortex Hamiltonian has no known division into integrable and small nonintegrable parts.

Apart from being an interesting dynamical system, a collection of point vortices is a widely used model in fluid mechanics. Numerical simulations of two-dimensional decaying turbulence, for example, show the appearance of self-organized coherent vortices. These vortices are relatively long lived, being destroyed or transformed in close encounters with other coherent vortices.[5] When such coherent vortices are far apart, their nearly conservative behavior may be approximated by a collection of point vortices. Indeed, remarkable agreement has been shown for relatively short times between a full numerical simulation and integration of 17 point vortices.[6]

The dynamics of point vortices has previously been studied in open domains and closed domains with reflecting walls,[4,7–14] but not in a domain with periodic boundary conditions. In an open domain one must restrict the vortices to having a single sign if one wishes to study long-time dynamics, since opposite-sign vortices tend to pair up and propagate off to infinity. A periodic domain does not have this difficulty. In addition, the chosen boundary conditions allow us to make contact with numerical simulations of two-dimensional fluids, calculations which have most often been made in a periodic domain.

A system is ergodic if ensemble averages equal time averages over any single trajectory, except a set of trajectories with measure zero. The ensemble average is over a surface defined by the constants of the motion. One difficulty with any numerical test of ergodicity is that ergodicity is defined in the limit where the number of elements in the ensemble and the duration of the time average approach infinity. In practice, however, it is only necessary to use samples large enough for equilibrium to be reached. But, there is always the possibility that what appears to be equilibrium is only metastable, or changes very slowly, and much larger samples are needed to reach true equilibrium.

The numerical study of ergodicity in near-integrable Hamiltonians dates back to Fermi *et al.*,[15] with recent work by Thirumalai and Mountain,[16] and Pettini and Landolfi.[17] In these studies, ergodicity is probed by investigating equipartition of energy. The dynamics of such systems displays a so-called stochasticity threshold: Energies above the threshold quickly reach equipartition, while those below the

 0899-8213/91/050835-10$02.00

threshold do not reach equipartition or do so very slowly. Here we investigate ergodicity in a fully nonintegrable Hamiltonian by direct comparison of ensemble and time averages. One mechanism for nonergodicity found in condensed matter physics[18] and two-dimensional magnetohydrodynamics[19] is that of symmetry breaking, where the equations of motions have a symmetry that is broken by their solutions. In this case, the phase space is broken into several components that are related by symmetry. Symmetry breaking is also found in a model of a negative temperature guiding-center plasma in a bounded circular domain, a system analogous to point vortices in the same domain.[20]

We also address the question of whether the chaotic motion of point vortices is similar to the motion of independent random walkers. This question arises because it is tempting to model coherent vortices in a fluid as a collection of randomly moving vortices whose interaction has a short spatial range. Such a model can only be correct if the chaotic motion mimics a random walk.

Section II of this paper contains a derivation of the equations of motion for point vortices in a periodic domain. In Sec. III, vortex pair statistics are used to investigate the qualitative behavior of vortex pairs, and to test the ergodicity and randomness of the chaotic motion.

II. POINT VORTICES IN A PERIODIC DOMAIN

The equations of motion for N point vortices in an infinite two-dimensional domain are[4]

$$\begin{pmatrix}\dot{x}_i\\ \dot{y}_i\end{pmatrix}=\frac{1}{2\pi}\sum_{j=1}^{N}{}'\frac{\kappa_j}{r_{ij}^2}\begin{pmatrix}-y_{ij}\\ x_{ij}\end{pmatrix}, \tag{1}$$

where (x_i,y_i) is the position of vortex i, κ_i is its circulation, $x_{ij}=x_i-x_j$, $y_{ij}=y_i-y_j$, $r_{ij}^2=x_{ij}^2+y_{ij}^2$, and the prime on the sum means to exclude the term $j=i$. We shall focus on the case $|\kappa_i|=\kappa$ for all i.

The equations of motion in a doubly periodic square domain are obtained by summing over the infinite number of image vortices produced by the boundary. By choosing an appropriate unit of distance the box size can be scaled to 2π, resulting in

$$\begin{pmatrix}\dot{x}_i\\ \dot{y}_i\end{pmatrix}=\frac{1}{2\pi}\sum_{j=1}^{N}{}'\kappa_j\begin{pmatrix}-S(y_{ij},x_{ij})\\ S(x_{ij},y_{ij})\end{pmatrix}, \tag{2}$$

where

$$S(x,y)=\sum_{m,n=-\infty}^{\infty}\frac{x-2\pi n}{(x-2\pi n)^2+(y-2\pi m)^2}. \tag{3}$$

In Eq. (3), the sum over m is absolutely convergent, while the sum over n is conditionally convergent. The dependence of S on the manner in which the limits are taken is seen by considering the finite sum

$$S_{M,N}(x,y)=\sum_{m=-M}^{M}\sum_{n=-N}^{N}\frac{x-2\pi n}{(x-2\pi n)^2+(y-2\pi m)^2}. \tag{4}$$

Using the method of Laplace transforms[21] on the sum over n, treating resulting integrals involving M and N asymptotically, and then taking the limit $M,N\to\infty$ only for those terms that are independent of the order of the limit results in

$$S_{M,N}=\sum_{m=-\infty}^{\infty}\frac{1}{2}\frac{\sin(x)}{\cosh(y-2\pi m)-\cos(x)}+\frac{x}{2\pi}-\frac{x}{\pi^2}\tan^{-1}\left(\frac{N}{M}\right). \tag{5}$$

The ratio N/M must now be chosen on physical grounds. We require that contributions to the velocity from equidistant image vortices cancel. Thus, the y velocity induced on vortex i from vortex j with $x_{ij}=\pi$ is zero, i.e., $S(\pi,y)=0$; this implies that the physically correct limit is

$$S(x,y)=\lim_{M\to\infty}\left[\lim_{N\to\infty}S_{M,N}(x,y)\right]=\sum_{m=-\infty}^{\infty}\frac{1}{2}\frac{\sin(x)}{\cosh(y-2\pi m)-\cos(x)}. \tag{6}$$

The result (6) is particularly useful as the remaining sum rapidly converges. By choosing an appropriate unit of time we can absorb the constants coming from (1) and (6) and rescale κ to unity. The final result for the equations of motion is

$$\begin{pmatrix}\dot{x}_i\\ \dot{y}_i\end{pmatrix}=\sum_{j=1}^{N}{}'\kappa_j\sum_{m=-\infty}^{\infty}\begin{pmatrix}\dfrac{-\sin(y_{ij})}{\cosh(x_{ij}-2\pi m)-\cos(y_{ij})}\\ \dfrac{\sin(x_{ij})}{\cosh(y_{ij}-2\pi m)-\cos(x_{ij})}\end{pmatrix}, \tag{7}$$

with $\kappa_i=\pm 1$.

We define a Hamiltonian H in terms of a vortex pair energy h,

$$H=-\sum_{ij}{}'\frac{\kappa_i\kappa_j}{2}h(x_{ij},y_{ij}), \tag{8}$$

such that

$$\kappa_i\begin{pmatrix}\dot{x}_i\\ \dot{y}_i\end{pmatrix}=\begin{pmatrix}\partial H/\partial y_i\\ -\partial H/\partial x_i\end{pmatrix}. \tag{9}$$

It is clear from the $\dot{x}$ part of (7) that

$$h(x,y)=\sum_{m=-\infty}^{\infty}\ln[\cosh(x-2\pi m)-\cos(y)]+f(x)+C. \tag{10}$$

The function f may be found by reconsidering the calculation leading to (6). Applying the Laplace transform to the sum over m instead of n we obtain

$$S(x,y)=\sum_{n=-\infty}^{\infty}\frac{1}{2}\frac{\sinh(x-2\pi n)}{\cosh(x-2\pi n)-\cos(y)}-\frac{x}{2\pi}. \tag{11}$$

Writing the equations of motion using (11) rather than (6) gives $f(x)=-x^2/2\pi$. Subtracting the (infinite) constant $\Sigma_m\ln[\cosh(2\pi m)]$ renders h finite (for $x^2+y^2\neq 0$). The final result for the vortex pair energy in a periodic square domain is

$$h(x,y)=\sum_{m=-\infty}^{\infty}\ln\left(\frac{\cosh(x-2\pi m)-\cos(y)}{\cosh(2\pi m)}\right)-\frac{x^2}{2\pi}. \tag{12}$$

The function h is manifestly periodic in y. Periodicity in x can be shown by considering (12) with asymptotically large limits in the sum and letting $x \to x + 2\pi$. The equality of (6) and (11) implies that the partial derivatives of $h(x,y)$ equal those of $h(y,x)$ from which one deduces that h is invariant under $x \rightleftharpoons y$.

Using the Hamiltonian, the equations of motion can be written in terms of a Poisson bracket,

$$\dot{x}_i = [x_i, H], \quad \dot{y}_i = [y_i, H], \tag{13}$$

with the Poisson bracket defined as

$$[f,g] \equiv \sum_{j=1}^{N} \frac{1}{\kappa_j} \left(\frac{\partial f}{\partial x_j} \frac{\partial g}{\partial y_j} - \frac{\partial f}{\partial y_j} \frac{\partial g}{\partial x_j} \right). \tag{14}$$

Consideration of sums of periodic images like those above has a history going back to Ewald,[22] and includes work by Nijboer and De Wette,[23] and Seyler.[24] More recently, following Nijboer and De Wette, Benzi and Legras[25] calculated the energy for a square periodic domain in terms of the exponential integral. Campbell, *et al.*[26] calculated the energy for more general periodic lattices; with some algebra it can be shown that the result (12) agrees, apart from an additive constant, with their result. O'Neil[27] derived the velocity in terms of the Weierstrass zeta function, the energy in terms of Jacobi theta functions, and verified numerically that his energy agreed with that of Campbell *et al.* The results presented above were derived independently, in a manner different from previous work, and are new. Due to rapid convergence of the remaining sums, the equations presented here are, like those obtained earlier, useful for numerical integration.

Point vortices in an infinite domain have four constants of the motion arising from the four symmetries of translation in time, translation in x and y, and rotation.[4] The periodic boundary conditions break the continuous rotation symmetry, leaving three constants of the motion. These are the energy $E = H(\{\kappa_i, x_i, y_i\})$, and the quantities $P_x = \Sigma_i \kappa_i y_i$ and $P_y = -\Sigma_i \kappa_i x_i$. We shall refer to $\mathbf{P} = P_x \hat{x} + P_y \hat{y}$ as the "vortex momentum"; it is related to the fluid momentum in a manner depending on the boundary conditions. The vortex momentum is discussed in further detail in the Appendix. As in the open domain, P_x and P_y are independent, i.e., have zero Poisson bracket, only if the total circulation $\Sigma_i \kappa_i$ is zero. For the remainder of this paper we shall assume that this is the case. Thus, we expect that three vortices are integrable, while four or more vortices are in general nonintegrable. Since we assume the vortices have circulations of equal magnitude and zero total circulation, N must be even.

The motion of N point vortices in a square periodic domain is thus a $2N$-dimensional Hamiltonian dynamical system. Using the canonical transformations found in Eckhardt and Aref,[14] the conserved vortex momentum can be used to reduce the dynamics to a phase space with four fewer dimensions. In this reduced phase space the only conserved quantity is the energy. Such reduction is particularly useful when the reduced phase space is small enough to be easily visualized, but comes at the expense of using nonphysical coordinates.

For four vortices, the reduced phase space is four dimensional; this is the well-studied case of low-dimensional Hamiltonian chaos and the usual features should appear. The case of four vortices in nonperiodic domains has been previously studied,[4,13,14] and the behavior is as expected. In particular, KAM curves can divide the phase space causing nonergodic behavior.

In this paper we are interested in the properties of higher-dimensional Hamiltonian chaos. We shall thus take the next step towards truly high-dimensional chaos and study the case of six vortices. The phase space is now 12 dimensional and can be reduced to eight dimensions. An eight-dimensional phase space, however, is not appreciably easier to deal with than a 12-dimensional phase space, and further, the coordinates become complicated. We thus choose to remain in the original phase space where the coordinates are the vortex positions.

III. DYNAMICS OF SIX POINT VORTICES

In this section we shall use the equations of motion derived above to numerically investigate the moderate dimensional chaos of six point vortices. The vortices reside in a square doubly periodic domain, have individual circulations of equal magnitude, and have zero total circulation. As discussed above, the dynamics has three constants of the motion: the energy and the two components of the vortex momentum. In this work we shall set the vortex momentum to zero, and study the effect on the dynamics of varying the energy. Note that $\mathbf{P} = 0$ is the average vortex momentum of an ensemble of randomly chosen vortex positions.

A qualitative picture of the effect of varying the energy can be obtained by heuristically considering the behavior of vortex pairs. A close pair of opposite-sign vortices has a large negative energy and will translate across the domain. A close pair of same-sign vortices has a large positive energy and will rotate about its center of vorticity. Thus, negative energy states will have opposite-sign pairs closer together than on average. The close opposite-sign pairs will translate across the domain and quickly "collide" with other vortices, resulting in scattering. By "collide" it is meant that the vortices become close enough that their interaction becomes significant. Thus, opposite-sign pairs will have a relatively short lifetime. On the other hand, positive energy states will have same-sign pairs closer together than on average. Since these pairs rotate but do not translate, they are only disrupted when another vortex comes nearby. As the energy increases, the same-sign pairs move closer together, making it less likely that another vortex will come close enough to disrupt them. Thus, we expect same-sign pairs to have a relatively long lifetime, with the lifetime increasing with energy.

It is easy to choose a random configuration on the $\mathbf{P} = 0$ surface due to the linearity of the vortex momentum. Indeed, one can prove by induction that if the strengths of all N vortices are known, the positions are restricted to $[0,2\pi]$, and the x positions of the first $m-1$ vortices are known, then $P_y = 0$ can only be satisfied provided x_m is chosen in the range

$$-(N-m-1)\pi - \kappa_m (q_{m-1} + s_{m-1}) \leqslant x_m \leqslant (N-m+1)\pi - \kappa_m (q_{m-1} + s_{m-1}), \tag{15}$$

where $q_n \equiv \Sigma_{i=1}^{n} \kappa_i x_i$, and $s_n = \pi \Sigma_{i=n+1}^{N} \kappa_i$. A similar rela-

tion holds for P_x and y_m. The relation (15) can be intuitively understood by thinking of the following analogous problem. Suppose one wants four numbers, two in [0,1] and two in [− 1,0], whose sum is zero. If after choosing the two positive numbers the sum is 1.8, then the third number must be in [− 1, − 0.8] for the four to sum to zero.

We shall use the relation (15) to choose random configurations subject to the constraint $P_x = P_y = 0$: Each position is chosen with uniform probability from the intersection of (15) and $[0,2\pi]$. Henceforth, when we speak of random configurations we shall mean subject to the above constraint.

We now ask the question: What is the probability that a random configuration with zero vortex momentum will have an energy in the range $(E,E + \Delta E)$? The answer is given by the density of states, $\rho(E,P_x = 0,P_y = 0)$. The density of states, plotted in Fig. 1, is calculated directly by choosing 10 000 random vortex configurations and counting the number within each energy range, and is normalized to unity. Both very high energies and very low energies are unlikely due to the small probability of two randomly placed vortices lying extremely close together. The density of states is a fundamental quantity in statistical mechanics, from which one can define an entropy S, and a temperature T,[28]

$$S = k \ln \rho, \quad \frac{1}{kT} = \frac{\partial S}{\partial E}. \tag{16}$$

Since states with positive energy have decreasing ρ, their temperature is negative.

While there has been previous work on the statistical mechanics of point vortices,[9,11,29] it differs from that presented in this paper in two important ways. First, numerical simulations were restricted to short times, while we find that very long times are needed to reach equilibrium. In addition, previous authors have made various assumptions common to statistical mechanics. Here the approach is to test such assumptions by direct integration of the equations of motion.

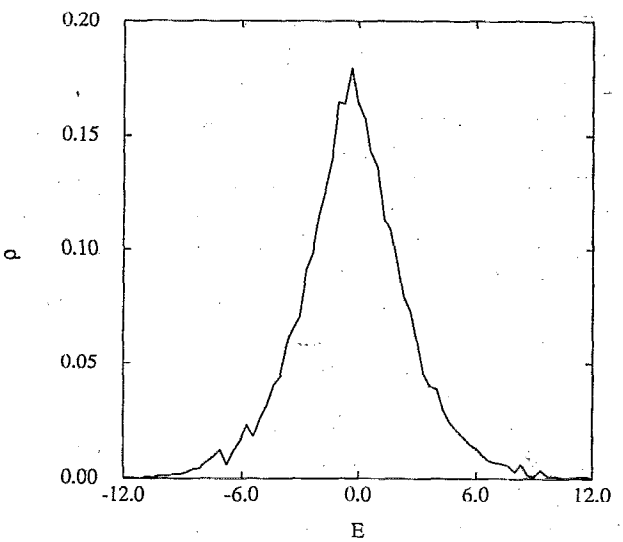

FIG. 1. Density of states vs energy for six vortices with $\mathbf{P} = 0$, calculated from 10 000 random configurations.

We shall focus on the dynamics at five different values of the energy. From the density of states the average and rms energies are found to be − 0.28 and 2.90, respectively. Joyce and Montgomery[10] calculate that ρ has its maximum at $E = 0$; here ρ peaks at a slightly negative energy. The small discrepancy is thought to be due to sampling error in our calculation of the density of states. The energy is rescaled by subtracting the value of the average energy from the original energy. Thus, energies above average are positive, and energies below average are negative. In addition, apart from complications due to the average energy being slightly displaced from the peak in ρ (also thought to be sampling error) positive energies have negative temperatures and vice-versa. The five energies to be investigated are the average energy ($\overline{E} = 0$), the average plus and minus 1 rms deviation, ($E_{\pm\sigma} = \pm 2.90$), and the average plus and minus 2 rms deviations ($E_{\pm 2\sigma} = \pm 5.80$).

The ensembles used for ensemble averages are collections of N_e random configurations with zero vortex momentum in an energy shell centered on the desired energy E. Configurations are randomly generated with arbitrary energy as described above and only those whose energy is within ΔE of E are included in the ensemble. It is found that ensemble averages are relatively insensitive to the range of energy allowed; in what follows a range of $\Delta E = 0.1$ was used. Alternatively, one could adjust the positions of vortices in the configurations until the required energy is reached; this technique, while not truly random, gives the same result as averaging over an energy shell for the cases tested.

To calculate time averages we start with an initial configuration with the desired energy. To obtain a given energy we generate random configurations with zero vortex momentum and arbitrary energy until a configuration is found whose energy is close to the required energy. Then, a vortex pair is chosen at random and their positions are adjusted until the required energy is reached.

Trajectories are generated from initial configurations by numerically integrating the equations of motion (7) on a Cray-XMP. The integration is done by the subroutine LSODE, a member of ODEPACK,[30] and is set to use a backward differentiation method. Owing to numerical errors neither the energy nor the vortex momentum are conserved exactly. For integrations of length $T = 100\,000$ time units the rms errors in the final energy and final components of the vortex momentum are 0.0487 and 7.33×10^{-7}, respectively. Although certain features of the dynamics, such as details about recurrences, are sensitive to exact conservation of invariants, the aspects considered here are not thought to be affected by these errors. Note that the errors in the energy are smaller than the width of the energy shell used for ensemble averages.

The numerical integrations generally confirm the qualitative view of point vortex dynamics described above. Vortex pairs of both signs are seen to be quite common and are often long lived. As expected, opposite-sign pairs quickly collide with either another vortex or a vortex pair. Quite often, however, rather than the pair being disrupted the result is an exchange of partners: the vortex pair continues but the identity of its members is different. In addition, clusters

of three and four vortices are visible, and, while not very common, can also be long lived. The long lifetime of larger clusters may be an intrinsic feature of such clusters or it may be due to the small number of remaining unclustered vortices.

Quantitative information about the dynamics is obtained by investigating vortex pair statistics. In particular, we calculate the average pair separation and two different two-particle distribution functions. The distribution functions are the standard two-particle distribution function $p(r)$, giving the probability of finding a vortex pair at a distance r,

$$p(r) = \langle \delta(r - r_{ij}) \rangle, \tag{17}$$

and the vorticity-weighted two-particle distribution function $q(r)$,

$$q(r) = \langle \kappa_i \kappa_j \delta(r - r_{ij}) \rangle. \tag{18}$$

In the above expressions the brackets indicate an average over all vortex pairs and either a time or ensemble average. Subscripts e and t will indicate ensemble and time averages, respectively. The distribution functions are normalized to correspond to those for a single opposite-sign vortex pair. Thus, the integral of $p(r)$ is normalized to one and the integral of $q(r)$ is normalized to negative one. Because the boundary conditions break the rotational symmetry we do not expect either $p(r,\theta)$ or $q(r,\theta)$ to be functions of r alone. However, the dependence on θ should be small for small r. In addition, by averaging over the angle, we reduce the uncertainties due to finite time integrations.

Pair distribution functions are well known in statistical mechanics and are often related to physically important quantities.[3] For point vortices, the time-averaged enstrophy spectrum can be calculated from q. The time-averaged enstrophy spectrum is defined as

$$S(\mathbf{k}) \equiv (1/2\pi) \langle |\zeta(\mathbf{k})|^2 \rangle, \tag{19}$$

where $\zeta(\mathbf{k})$ is the Fourier transform of the vorticity, and the brackets indicate a time average. For point vortices $\zeta(\mathbf{r}) = \Sigma_i \kappa_i \delta(\mathbf{r} - \mathbf{r}_i)$, from which one finds

$$S(\mathbf{k}) = q(\mathbf{k}) + (N/2\pi), \tag{20}$$

where $q(\mathbf{k})$ is the Fourier transform of $q(\mathbf{r})$. By integrating over the angle, one obtains

$$S(k) = q(k) + Nk, \tag{21}$$

where $q(k)/k$ is the Hankel transform of $q(r)/r$.

Together, the two distribution functions give complete information about vortex pairs. The probability of a same- or opposite-sign pair at a distance r is $[p(r) + / - q(r)]/2$. If $q(r)$ is zero then there are either no vortex pairs at a distance r or an equal number of same-sign and opposite-sign pairs; the two possibilities are distinguished by whether $p(r)$ is also zero.

Trajectories were integrated for $T = 100\,000$ starting from one initial condition at each of the five selected energies. Time averages were calculated from these trajectories by sampling every 0.2 time units. Since the time unit is defined in terms of κ, these trajectories are quite long on the scale of the vorticity. As the vorticity determines the scale of the velocity, the trajectories are also very long in terms of the distance a vortex travels and hence the number of close encounters with other vortices. One can define a two-vortex correlation time by calculating a correlation function for the two-vortex distribution function $p(r;t)$, where $p(r;t)$ is defined as the time averaged $p(r)$ obtained from the time interval $(t,t + 50)$. It is found that the correlation time is approximately 200 time units for $\overline{E}$, grows to 500 for $E_{-2\sigma}$, and to 2500 for $E_{+2\sigma}$. The correlation time increases with the magnitude of the energy due to long-lived pairs, with the larger increase at positive energies caused by the longer lifetime of same-sign pairs. Thus, the full trajectories are long compared to the two-vortex correlation time.

Ensemble averages are calculated from N_e random configurations whose energy is within 0.1 of the selected energy. For $\overline{E}$ and $E_{\pm\sigma}$ a value of $N_e = 200\,000$ was used, while for $E_{\pm 2\sigma}$ a value of $N_e = 50\,000$ was used. A smaller sample size was used at $E_{\pm 2\sigma}$ due to the low probability of finding a random configuration with such extreme energy and the resulting extensive searching required.

For both time and ensemble averages we estimate the errors due to using a finite sample size by subsampling. Each sample is broken into five subsamples of equal size. The uncertainty in the mean is then estimated as $\sigma/\sqrt{5}$, where σ^2 is the variance of the means obtained from the subsamples. The uncertainties are shown as error bars in Fig. 2, and as gray shaded regions in Figs. 3–7. Regions in Figs. 3–7 where the shading is not apparent have uncertainties smaller than the width of the line representing the mean.

In addition to testing ergodicity, we wish to compare the dynamics to the motion of independent random walkers. For a random walk, the time-averaged pair distribution functions are independent of the details of the process provided the random walkers are independent. Since independent

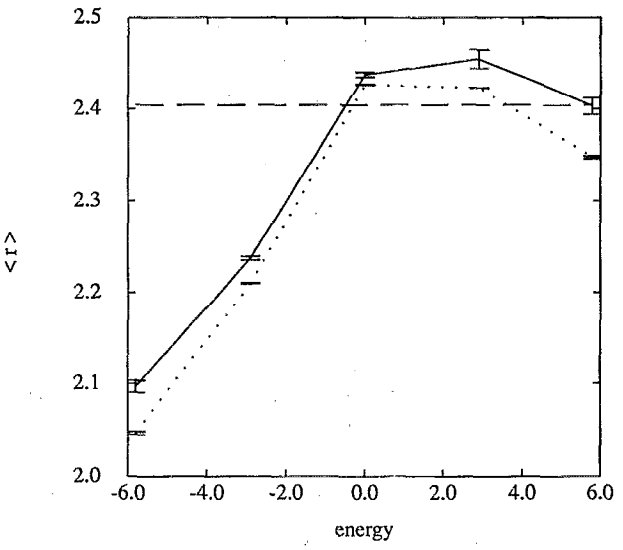

FIG. 2. Average vortex pair separation versus energy. The solid line denotes time average, the dotted line denotes ensemble average, and the dashed line denotes independent random walkers. Error bars are estimates of the uncertainty due to finite sample size.

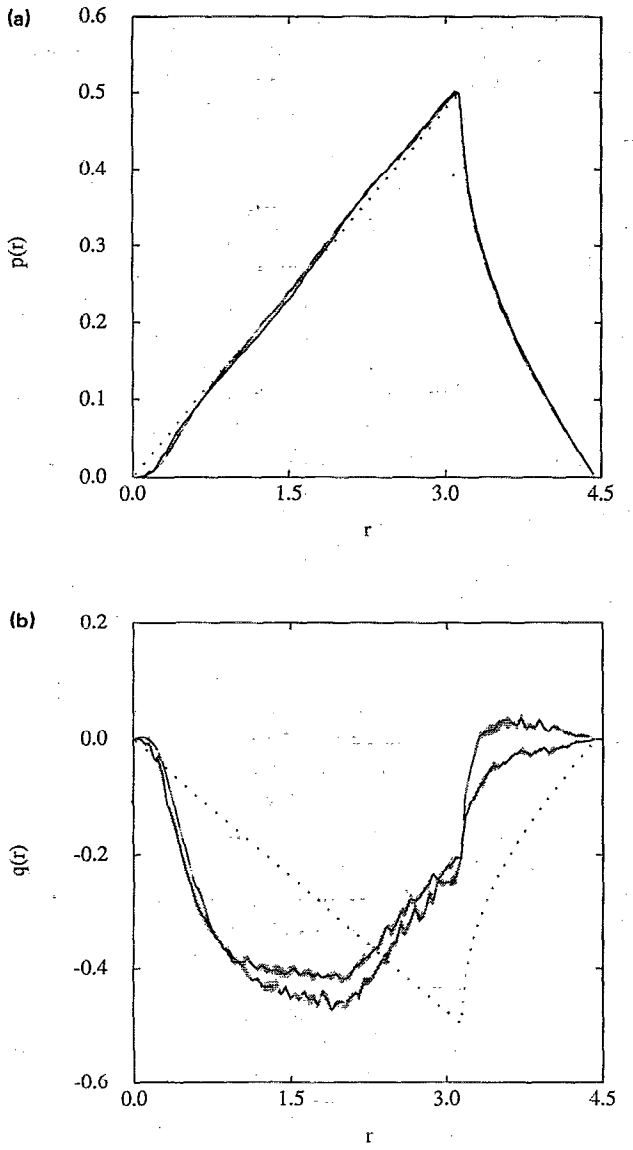

FIG. 3. (a) Two-particle distribution function $p(r)$ vs r for $E = \overline{E} = 0$. The solid, dashed, and dotted lines are time averages, ensemble averages, and independent random walkers, respectively. Gray stippled regions (which are very thin in this figure) are estimates of the uncertainty due to finite sample size. (b) Vorticity-weighted two-particle distribution function $q(r)$ vs r for $E = \overline{E} = 0$. Line types and shading are the same as (a).

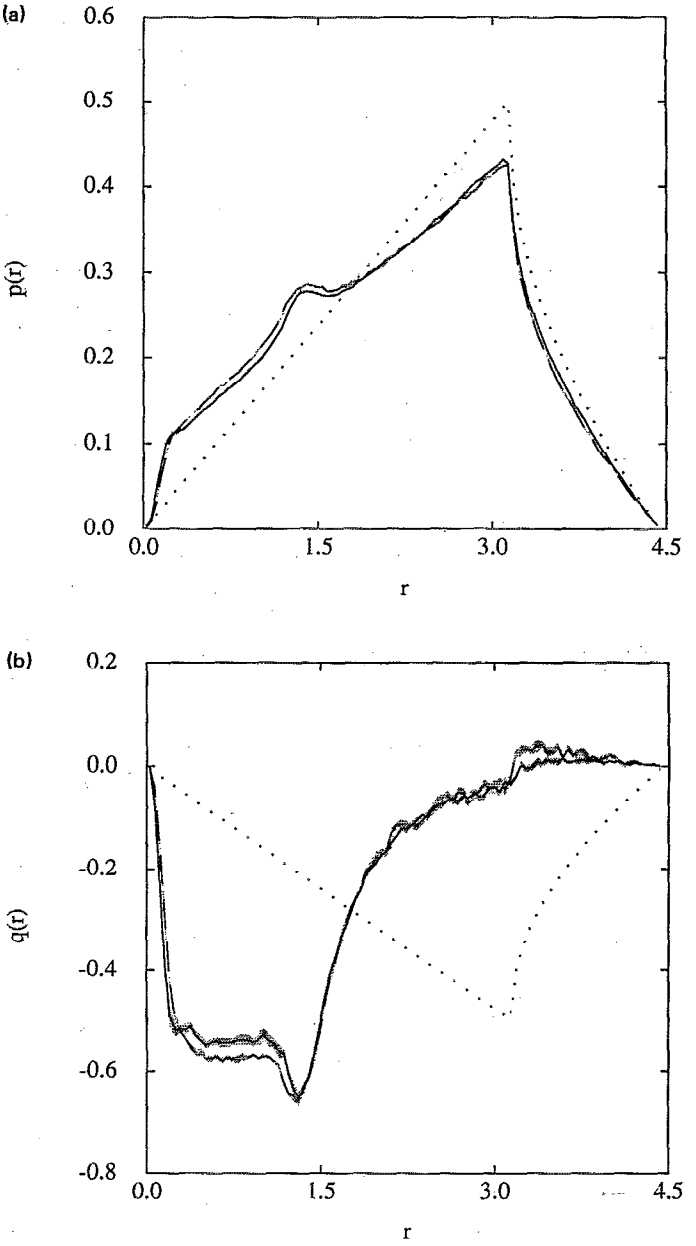

FIG. 4. (a) Same as Fig. 3(a) but $E = E_{-\sigma} = -2.90$. (b) Same as Fig. 3(b) but $E = E_{-\sigma} = -2.90$.

random walkers have equal probability of being separated by any vector **r**, their pair distribution functions are determined by the area at radius r in a square with sides of length 2π:

$$p_{\mathrm{rw}}(r) = \begin{cases} r/2\pi, & r \leqslant \pi, \\ r/2\pi - (2r/\pi^2)\cos^{-1}(\pi/r), & \pi \leqslant r \leqslant \sqrt{2}\pi. \end{cases} \tag{22}$$

For the case we are considering, N vortices, half with $\kappa_i = 1$ and half with $\kappa_i = -1$, there are $N/2$ more opposite-sign pairs than same-sign pairs. Thus, since $q(r)$ is normalized to the case $N = 2$,

$$q_{\mathrm{rw}}(r) = -p_{\mathrm{rw}}(r). \tag{23}$$

From (22) one obtains that the average pair separation of independent random walkers is

$$\langle r \rangle_{\mathrm{rw}} \equiv \int_0^{\pi\sqrt{2}} dr\, r p_{\mathrm{rw}}(r) = \frac{\pi\sqrt{2}}{3} + \frac{\pi}{3}\ln(1+\sqrt{2}). \tag{24}$$

The average vortex pair separation at the five selected energies is shown in Fig. 2. The solid, dotted, and dashed lines represent the results for the time average, ensemble average, and random walkers, respectively. The qualitative behavior of the two averages as a function of energy is similar but they are quantitatively distinct. For all energies the time-

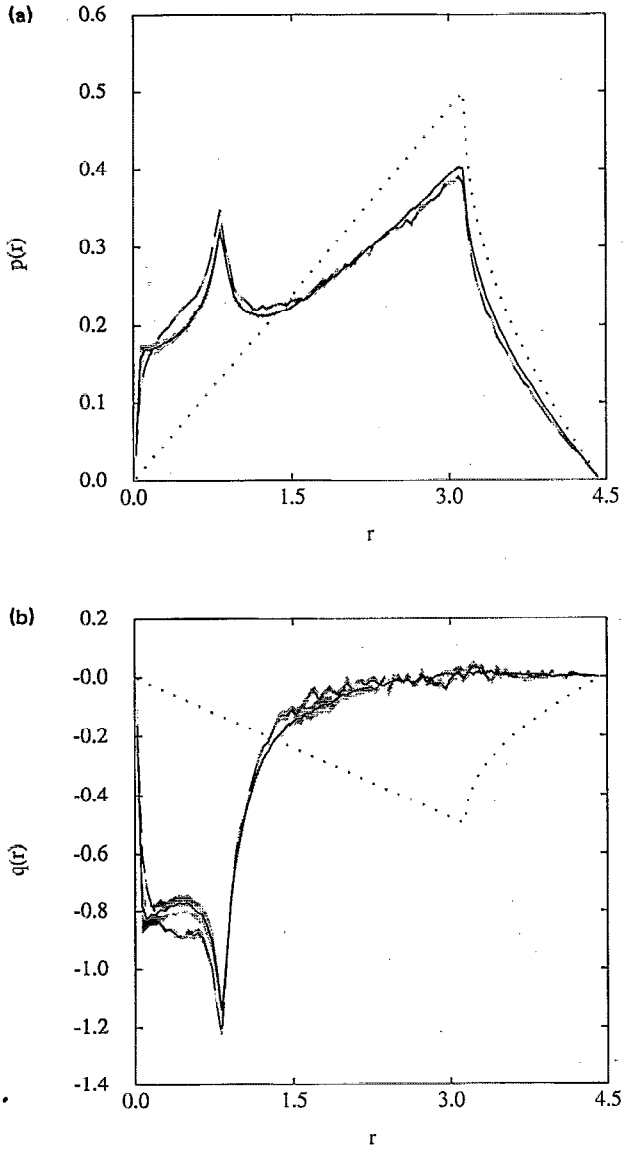

FIG. 5. (a) Same as Fig. 3(a) but $E = E_{-2\sigma} = -5.80$. (b) Same as Fig. 3(b) but $E = E_{-2\sigma} = -5.80$.

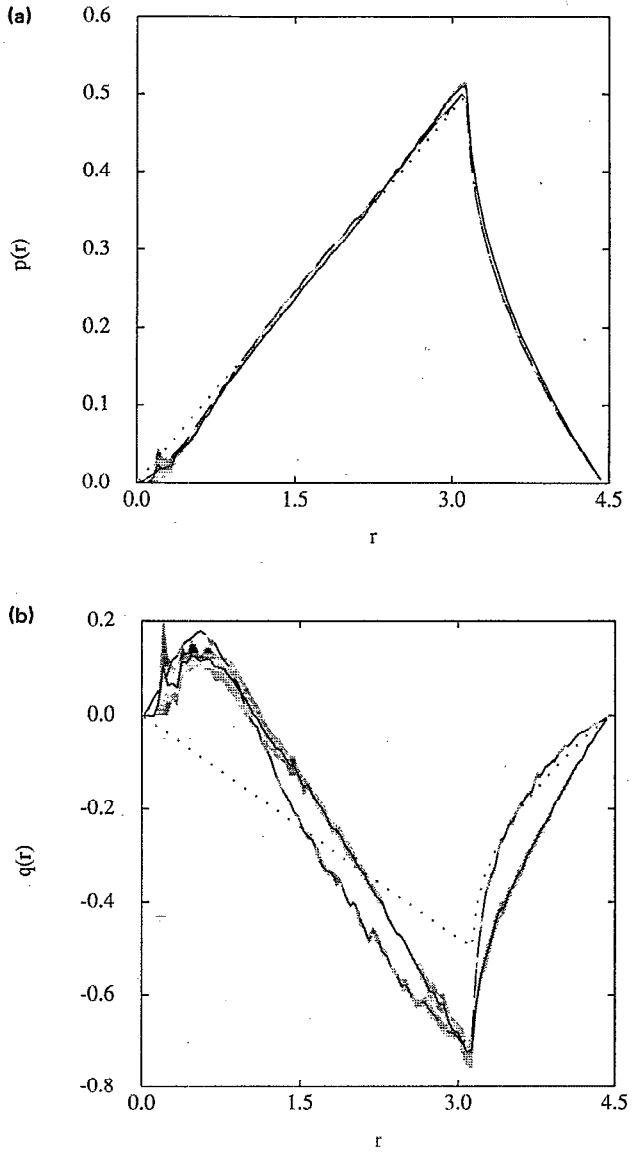

FIG. 6. (a) Same as Fig. 3(a) but $E = E_{+\sigma} = 2.90$. (b) Same as Fig. 3(b) but $E = E_{+\sigma} = 2.90$.

averaged pair separation is significantly larger than the ensemble average. The asymmetry about $E = 0$ is striking. For negative energies there is a sharp decrease in the average separation, while for positive energies, the average separation is almost constant. This asymmetry results from the asymmetry in the behavior of $p(r)$ discussed below. In addition, the time average differs significantly from that of random walkers at all but the largest energy.

The two-particle distribution functions are shown in Figs. 3–7. In these figures, the solid lines indicate time averages, dashed lines indicate ensemble averages, and dotted lines indicate random walkers. At all energies, the time and ensemble averages agree qualitatively but not quantitatively.

The results for the average energy, $E = \overline{E}$, are shown in Figs. 3(a) and 3(b). While p_t, p_e, and $p_{\rm rw}$ are similar [Fig. 3(a)], the differences are significant. In particular, both p_t and p_e display a dearth of very close pairs and an excess of medium-spaced pairs over $p_{\rm rw}$. The differences, however, are more apparent when the sign of the pairs is considered. From Fig. 3(b) it is seen that q_t and q_e are qualitatively similar and have considerably more opposite-sign close pairs and more same-sign distant pairs than random. Further, the ensemble average has more close opposite-sign pairs and more distant same-sign pairs than the time average. Also note the sharp change in behavior at $r = \pi$ where both q_t and q_e go from an excess of opposite-sign pairs to almost equal numbers of same-sign and opposite-sign pairs.

At an energy one rms deviation below the average, $E = E_{-\sigma}$ [Figs. 4(a) and 4(b)], the time-averaged and ensemble-averaged distributions again display a large number of opposite-sign close pairs and roughly the same number of same-sign and opposite-sign pairs at larger separations. The boundary between the two regimes is $r \simeq 2$. The distributions

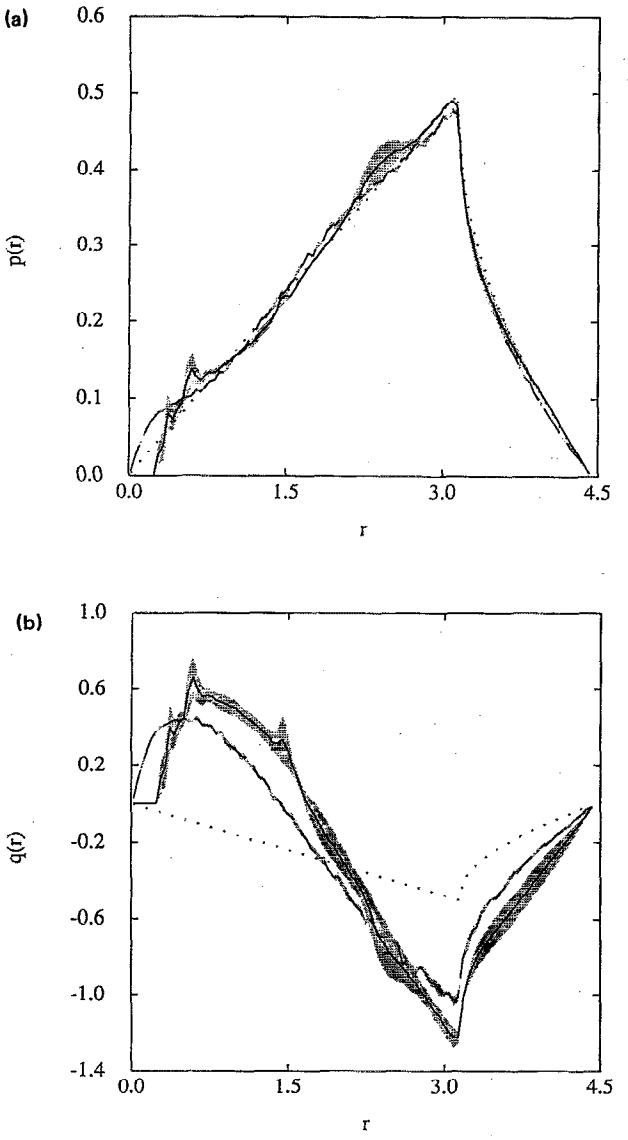

FIG. 7. (a) Same as Fig. 3(a) but $E = E_{+2\sigma} = 5.80$. (b) Same as Fig. 3(b) but $E = E_{+2\sigma} = 5.80$.

show the beginnings of a sharp peak at $r \simeq 1.3$. As was the case for the average energy, the ensemble average contains more close opposite-sign pairs than the time average. Both time- and ensemble-averaged p and q are distinctly different from random walkers.

The distributions at $E = E_{-2\sigma}$ [Figs. 5(a) and 5(b)] are similar to that at $E_{-\sigma}$: There is an enhanced probability of opposite-sign pairs at small distances, and equal probability of same-sign and opposite-sign pairs at larger distances. The boundary between the regimes, however, has changed, and is now at $r \simeq 1.3$. The peak visible at $E_{-\sigma}$ has become larger, sharper, and is now at $r \simeq 0.8$. As before, the ensemble average contains more close opposite-sign pairs than the time average, and both are very different than random walkers.

The behavior at positive energies is qualitatively different than at negative energies. At $E = E_{+\sigma}$, p_t and p_e [Fig. 6(a)] are similar to those at $\overline{E}$, while q_t and q_e [Fig. 6(b)] have changed significantly. There is now an excess of close same-sign pairs and distant opposite-sign pairs, but no evidence of a sharp peak. The ensemble average has more close same-sign pairs and more distant opposite-sign pairs than the time average.

The behavior at the extreme positive energy, $E = E_{+2\sigma}$, is similar to that at $E_{+\sigma}$, but the features are more pronounced [Figs. 7(a) and 7(b)]. Both p_t and p_e are now clearly not random, particularly at very small distances. The vorticity weighted distributions q_t and q_e again show a broad peak of same-sign pairs at small distances and opposite-sign pairs at large distances.

The fact that the uncertainties due to finite sample size are small indicates that the samples are generally large enough to have equilibrated. A general trend is that the uncertainties increase at more extreme energies. It is quite possible, however, that the distributions have not equilibrated at positive energies at very small distances. At both $E_{+\sigma}$ and $E_{+2\sigma}$, there are no pairs below a certain distance. It may be that such extremely close pairs would appear in longer time integrations. Even if this were the case, however, the differences between the time averages and the ensemble averages are large enough that they would probably not disappear entirely.

The question now arises as to the mechanism for the nonergodicity apparent in the data. In systems reducible to motion on a three-dimensional energy surface, KAM surfaces can produce nonergodicity by dividing the energy surface into separate components. In this case, trajectories resulting from initial conditions in different components produce different results. Thus, by calculating time averages over several trajectories from different initial conditions we can investigate whether the surface defined by the energy and vortex momentum is effectively broken into separate

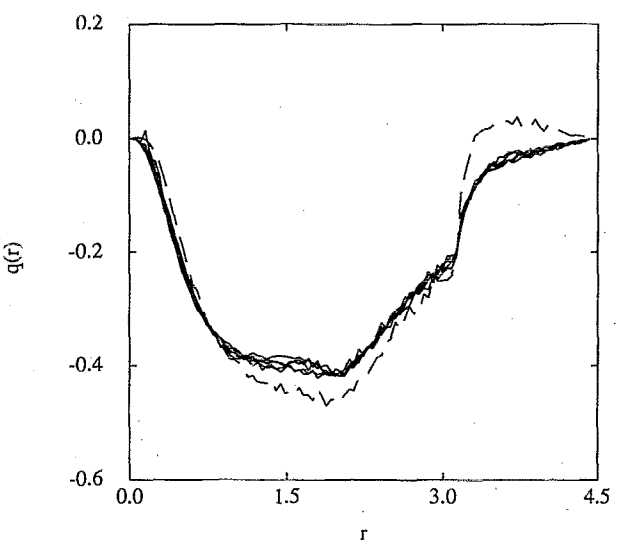

FIG. 8. Vorticity-weighted two-particle distribution function $q(r)$ vs r for $E = \overline{E} = 0$. The solid lines are time averages over each of five trajectories with different initial conditions. The dashed line is the ensemble average.

components. Five different random initial configurations, each with energy $E = \overline{E}$, were integrated for $T = 100\,000$ time units. The resulting vorticity-weighted distribution functions are shown in Fig. 8. Only q is plotted since p_t and p_e are similar at this energy. The five solid lines are the five different time averages, while the dashed line is the ensemble average. The five time averages agree to within roughly twice the uncertainty indicated in Fig. 3(b), and are distinctly different than the ensemble average. This indicates that the nonergodicity is not due to the energy-vortex momentum surface being broken into several components of roughly equal size. Due to the long time necessary for these integrations it was not possible to compute multiple trajectories at other energies.

IV. CONCLUSIONS

The differences between the dynamics at negative energies (positive temperatures) and at positive energies (negative temperatures) are several. As expected from qualitative considerations the positive energy states contain relatively more close same-sign pairs, while the negative energy states contain relatively more close opposite-sign pairs. For both positive and negative energies, there is enhanced vortex pairing as the magnitude of the energy increases, but the pairing takes qualitatively different forms.

Negative energy states display an increasingly sharp peak in the two-particle distribution functions as the magnitude of the energy increases, with the peak moving to smaller distances. This peak represents an enhanced probability of finding opposite-sign vortex pairs at a particular distance. This distance is not determined by a length scale external to the problem, but is chosen by the dynamics itself and depends on the energy. At larger vortex separations there are roughly equal probabilities of finding opposite-sign and same-sign pairs. A consequence of this behavior is that the average vortex pair separation decreases as the magnitude of the energy increases.

Positive energy states show an enhanced probability of close same-sign pairs which takes the form of a broad hump rather than a sharp peak. At larger distances there is an excess of opposite-sign pairs. This separation of close same-sign pairs and distant opposite-sign pairs results in the average pair separation remaining roughly constant with energy.

At all energies considered there are significant differences between the time-averaged and ensemble-averaged distribution functions. Thus, at least for the time scales considered here, the dynamics is not ergodic. These time scales are quite long and appear to be sufficient for the time average to equilibrate.

We now look into the mechanism for the nonergodicity. According to Birkhoff's theorem,[3,31] nonergodicity implies that the energy-vortex momentum surface is decomposable, i.e., it is broken into more than one component. We suspect, but have not confirmed, that Birkhoff's theorem holds here. If the nonergodicity is due to a broken symmetry, then the components have equal areas, since they are related by symmetry. The fact that five separate initial conditions converge to the same time average, different than the ensemble average, means that it is unlikely that the surface is broken into several equal-sized components. Thus the nonergodicity is probably not due to a broken symmetry. The remaining possibility is that there is one region covering a large part of the surface and one or more much smaller regions in the remainder. In this case, it is not unlikely that the five separate initial conditions were all in the same region. Since the calculations were necessarily finite time integrations, we cannot rule out the possibility that, rather than being truly separate components, the regions are separated by weakly permeable barriers, and hence the dynamics is ultimately ergodic. The length of the integrations, however, indicates that, if Arnold diffusion through such barriers is possible, it is extremely slow, and thus the time scale for ergodicity is very long. Identification of these regions and the dynamics of trajectories within them will be the subject of future work.

Finally, the chaotic behavior of point vortices is clearly distinct from the motion of independent random walkers. Thus, a model of two-dimensional turbulence in terms of randomly moving coherent vortices would not display the correct behavior.

ACKNOWLEDGMENTS

J.W. would like to thank M. Marder for interesting and useful discussions.

The National Center for Atmospheric Research is sponsored by the National Science Foundation.

APPENDIX: THE VORTEX MOMENTUM

In this appendix we address two aspects of the "vortex momentum,"

$$\mathbf{P} \equiv \sum_i \kappa_i (y_i \hat{x} - x_i \hat{y}) \equiv -\sum_i \kappa_i \hat{k} \times \mathbf{x}_i. \tag{A1}$$

First, we show that the conservation of $\mathbf{P}$ is due to translation symmetry, and second, we show that $\mathbf{P}$ is equal to the fluid momentum, $\mathscr{P} \equiv \int\int_0^{2\pi} d^2\mathbf{x}\ \mathbf{u}$, plus a boundary term.

The imposition of periodic boundary conditions breaks the rotation symmetry present in an open domain. The translation symmetries do remain, however, and result in the conservation of the vortex momentum. The translation symmetry is reflected in the functional form of the vortex pair energy in a periodic domain: $h(\mathbf{x}_i, \mathbf{x}_j) = h(\mathbf{x}_{ij})$. Further, one sees that the rotation symmetry of the open domain is broken by the fact that h is not a central potential: $h(\mathbf{x}_{ij}) \neq h(|\mathbf{x}_{ij}|)$. Using the Poisson bracket defined in Eq. (14) above, it is straightforward to show that $d\mathbf{P}/dt = [\mathbf{P}, H]$ is made up of sums of terms of the form $\partial h(\mathbf{x}_{ij})/\partial x_i + \partial h(\mathbf{x}_{ij})/\partial x_j = 0$. Thus, conservation of $\mathbf{P}$ is due to the translation symmetry of h.

The relationship of $\mathbf{P}$ to the fluid momentum $\mathscr{P}$ is best addressed by considering the analog to the vortex momentum for a continuous distribution of vorticity $\zeta(\mathbf{x})$. From the definition of $\mathbf{P}$, Eq. (A1) above, we see that $\mathbf{P}$ is a Lagrangian quantity: The individual vortices are followed through time preserving their strengths κ_i, and $\mathbf{P}$ is calculated using their current position $\mathbf{x}_i$. Also note that in Eq. (A1) the positions of the vortices are not restricted to the basic square, $x, y \in (0, 2\pi)$. It is clear from Eq. (A1) that $\mathbf{P}$ is not invariant under the transformation $\mathbf{x}_i \to \mathbf{x}_i + 2\pi n\hat{x} + 2\pi m\hat{y}$.

Thus, $\mathbf{P}$ can only be time independent if the vortices are allowed to evolve freely, and are not mapped back into the basic square when they leave. The dynamics, governed by Eq. (7) above, is invariant under the transformation, and does not distinguish between whether or not the vortices are mapped back to the basic square.

Thus, to find the correct analog of the vortex momentum for continuously distributed vorticity, we imagine starting the fluid with a specified vorticity in the basic square, and then following the Lagrangian evolution of the fluid parcels. The position of a parcel at time t which was initially at $\mathbf{x}$ is denoted by $\mathbf{X}(t;\mathbf{x})$. Since vorticity doesn't change following parcels,

$$\mathbf{P} \equiv -\int\int_0^{2\pi} d^2\mathbf{x}\, \hat{k} \times \mathbf{X}(t;\mathbf{x})\zeta(\mathbf{x}) \tag{A2a}$$

$$= -\int\int_0^{2\pi} d^2\mathbf{x}\, \hat{k} \times \mathbf{X}(t;\mathbf{x})\zeta[\mathbf{X}(t;\mathbf{x})] \tag{A2b}$$

$$= -\int\int_D d^2\mathbf{X}\, \hat{k} \times \mathbf{X}\zeta(\mathbf{X}), \tag{A2c}$$

where D denotes the region into which the basic square has evolved at time t. The Lagrangian evolution of the basic square into D is an area-preserving rearrangement of the fluid parcels. This implies that each point $\mathbf{X} \in D$ can be mapped back to the basic square by a translation of $2\pi m(\mathbf{X})\hat{x} + 2\pi n(\mathbf{X})\hat{y}$ such that the image of D is exactly the basic square. Thus, an integral over D of a periodic quantity is equivalent to an integral over the basic square. Eq. (A2) should be contrasted with the Eulerian expression

$$\mathbf{P}_E \equiv -\int\int_0^{2\pi} d^2\mathbf{x}\, \hat{k} \times \mathbf{x}\zeta(\mathbf{x},t).$$

In either a closed or a nonperiodic open domain the integrals would be over the entire fluid, and since the transformation between $\mathbf{x}$ and $\mathbf{X}(t;\mathbf{x})$ amounts to an area-preserving rearrangement of the fluid parcels, the two expressions would be equal. In a periodic domain, however, the integrals are only over D and the basic square, and the two expressions may differ.

We now show that the vortex momentum can be expressed as a sum of the fluid momentum and a boundary term. For simplicity we consider only the x component P_x; the y component is handled similarly. For a continuous distribution of vorticity, $\zeta = \hat{k}\cdot(\nabla\times\mathbf{u})$, Eq. (A2c) then gives

$$P_x = \int\int_D d^2\mathbf{X}\; Y\hat{k}\cdot[\nabla\times\mathbf{u}(\mathbf{X})]$$

$$= \int\int_D d^2\mathbf{X}\; \hat{k}\cdot[\nabla\times(Y\mathbf{u}) + (\mathbf{u}\cdot\hat{x})\hat{k}\,],$$

$$= \int_{\partial D} d\mathbf{s}\cdot\mathbf{u}Y + \int\int_D d^2\mathbf{X}\; \mathbf{u}\cdot\hat{x},$$

where the final line results from Stokes' theorem. Thus,

$$P_x = \int_{\partial D} d\mathbf{s}\cdot\mathbf{u}Y + \mathscr{P}_x. \tag{A3}$$

The first term in Eq. (A3) is the boundary term mentioned above, while the second term is the x component of the fluid momentum per unit square. Note that in the case of a nonperiodic open domain where $\mathbf{u}$ falls off faster than $1/r$, the boundary term goes to zero and $\mathbf{P} = \mathscr{P}$.

[1] A. J. Lichtenberg and M. A. Lieberman, *Regular and Stochastic Motion* (Springer-Verlag, New York, 1983).
[2] R. S. Mackay and J. D. Meiss, *Hamiltonian Dynamical Systems* (Adam Hilger, Bristol, 1987).
[3] R. Balescu, *Equilibrium and Nonequilibrium Statistical Mechanics* (Wiley, New York, 1975).
[4] H. Aref, Annu. Rev. Fluid Mech. **15**, 345 (1983).
[5] J. C. McWilliams, J. Fluid Mech. **219**, 361 (1990).
[6] R. Benzi, S. Patarnello, and P. Santangelo, J. Phys. A **21**, 1221 (1988).
[7] G. R. Kirchhoff, *Vorlesungen über Matematische Physik* (Teubner, Leipzig, 1876), Vol. 1.
[8] C. C. Lin, *On the Motion of Vortices in Two Dimensions* (University of Toronto Press, Toronto, 1943).
[9] L. Onsager, Nuovo Cimento Suppl. **6**, 279 (1949).
[10] G. Joyce and D. Montgomery, J. Plasma Phys. **10**, 107 (1973).
[11] D. Montgomery and G. Joyce, Phys. Fluids **17**, 1139 (1974).
[12] R. H. Kraichnan and D. Montgomery, Rep. Prog. Phys. **43**, 547 (1980).
[13] H. Aref and N. Pomphrey, Proc. R. Soc. London Ser. A **380**, 359 (1982).
[14] B. Eckhardt and H. Aref, Philos. Trans. R. Soc. London Ser. A **326**, 655 (1988).
[15] E. Fermi, J. Pasta, and S. Ulam, in *Collected Papers of Enrico Fermi* (University of Chicago Press, Chicago, 1965), Vol. II, p. 978.
[16] D. Thirumalai and R. D. Mountain, J. Stat. Phys. **57**, 789 (1989).
[17] M. Pettini and M. Landolfi, Phys. Rev. A **41**, 768 (1990).
[18] R. G. Palmer, Adv. Phys. **31**, 669 (1982).
[19] J. V. Shebalin, Physica D **37**, 173 (1989).
[20] R. A. Smith, Phys. Rev. Lett. **63**, 1479 (1989).
[21] A. D. Wheelon, *Tables of Summable Series and Integrals Involving Bessel Functions* (Holden-Day, San Francisco, 1968), p. 3.
[22] P. P. Ewald, Ann. Phys. (Leipzig) **64**, 253 (1921).
[23] B. R. A. Nijboer and F. W. De Wette, Physica (Utrecht) **23**, 309 (1957).
[24] C. E. Seyler, Jr., Phys. Rev. Lett. **32**, 515 (1974); Phys. Fluids **19**, 1336 (1976).
[25] R. Benzi and B. Legras, J. Phys. A **20**, 5125 (1987).
[26] L. J. Campbell, M. M. Doria, and J. B. Kadtke, Phys. Rev. A **39**, 5436 (1989).
[27] K. A. O'Neil, in *Mathematical Aspects of Vortex Dynamics*, edited by R. E. Caflisch (SIAM, Philadelphia, 1989).
[28] R. P. Feynman, *Statistical Mechanics* (Benjamin/Cummings, Reading, MA, 1972).
[29] T. S. Lundgren and Y. B. Pointin, J. Stat. Phys. **17**, 323 (1977).
[30] A. C. Hindmarsh, in *Scientific Computing*, edited by R. S. Stepleman in collaboration with M. Carver, R. Peskin, W. F. Ames, and R. Vichnevetsky (North-Holland, Amsterdam, 1983), p. 55.
[31] A. I. Khinchin, *Mathematical Foundations of Statistical Mechanics* (Dover, New York, 1949).